Tissue Eng Regen Med (2020) 17(4):433–443
https://doi.org/10.1007/s13770-020-00260-w

Online ISSN 2212-5469

ORIGINAL ARTICLE

# Development of Acellular Respiratory Mucosal Matrix Using Porcine Tracheal Mucosa

**Soo Yeon Jung[1] · An Nguyen-Thuy Tran[1] · Ha Yeong Kim[1,2] · Euno Choi[3] · So Jeong Lee[1] · Han Su Kim[1]**

Received: 2 December 2019 / Revised: 2 April 2020 / Accepted: 3 April 2020 / Published online: 10 May 2020


**Abstract**

***BACKGROUND:*** Respiratory mucosa defects result in airway obstruction and infection, requiring subsequent functional recovery of the respiratory epithelium. Because site-specific extracellular matrix (ECM) facilitates restoration of organ function by promoting cellular migration and engraftment, previous studies considered decellularized trachea an ideal ECM; however, incomplete cell removal from cartilage and mucosal-architecture destruction are frequently reported. Here, we developed a decellularization protocol and applied it to the respiratory mucosa of separated porcine tracheas.

***METHODS:*** The trachea was divided into groups according to decellularization protocol: native mucosa, freezing–thawing (FT), FT followed by the use of Perasafe-based chemical agents before mucosal separation (wFTP), after mucosal separation (mFTP), and followed by DNase decellularization (mFTD). Decellularization efficacy was evaluated by DNA quantification and hematoxylin and eosin staining, and ECM content of the scaffold was evaluated by histologic analysis and glycosaminoglycan and collagen assays. Biocompatibility was assessed by cell-viability assay and *in vivo* transplantation.

***RESULTS:*** The mFTP mucosa showed low antigenicity and maintained the ECM to form a proper microstructure. Additionally, tonsil-derived stem cells remained viable when cultured with or seeded onto mFTP mucosa, and the *in vivo* host response showed a constructive pattern following implantation of the mFTP scaffolds.

***CONCLUSION:*** These results demonstrated that xenogenic acellular respiratory mucosa matrix displayed suitable biocompatibility as a scaffold material for respiratory mucosa engineering.

**Keywords** Respiratory mucosa · Porcine · Trachea · Decellularization · Biocompatible scaffold

## 1 Introduction

The respiratory tract (nasal cavity–pharynx–larynx–trachea–bronchus) allows the passage of air. The mechanical properties of this tract prevent collapse during inspiration–expiration, and its biological properties provide immunological defense. Among the structures constituting the respiratory tract, bone, and cartilage are responsible for the mechanical features, and the respiratory epithelium is important for its biological characteristics. A clinical defect in the respiratory tract is treated by primary repair or resection of the diseased area and anastomosis of the

✉ Han Su Kim
sevent@ewha.ac.kr

[1] Department of Otorhinolaryngology - Head and Neck Surgery, College of Medicine, Ewha Womans University, Anyangcheon-ro 1071, Yang Cheon-Gu, Seoul 07985, Korea

[2] Department of Molecular Medicine, College of Medicine, Ewha Womans University, Seoul 07985, Korea

[3] Department of Pathology, College of Medicine, Ewha Womans University, Seoul 07985, Korea

healthy area; however, for large defects, transplantation of the organ might be the only treatment option.

Development of airway scaffold, which provides the template for tissue regeneration and facilitate the cellular engraftment, was new treatment option for respiratory tract defect. Previous studies describe development of tracheal and bronchial scaffold from the respiratory tract using multiple methods [1–19]. Scaffold fabricated from synthetic materials are easily produced and show excellent restorative mechanical properties and proper microstructure [1, 4–6, 8, 11, 20, 21]; however, when reconstructing the entire airway, improper biological function results in mucus pooling and crust formation. Site-specific extracellular matrix (ECM) facilitates restoration of organ function by improving cellular migration and engraftment. Previous studies described the use of numerous biologically derived ECMs to restore this function [13–19, 22, 23]. To reduce immunological rejection and facilitate functional recovery, a proper decellularization method for removing all donor cells and simultaneously preserving the ECM and structure is required. Balancing these two goals is the greatest current limitation to organ decellularization, particularly when this organ comprises different tissue types. Most of the respiratory tract comprises cartilage and mucosa, which histologically constitutes pseudocolumnar ciliated epithelium that performs immunological functions, such as mucus secretion from goblet cells and transport by ciliary movement. Exposure of this tissue to decellularizing agents for an extended period results in massive destruction of the ECM and structure, leading to failed functional recovery. By contrast, cartilage is resistant to decellularizing agents [15, 17, 18], although remaining DNA content results in immunological rejection. Accordingly, it is difficult to remove cells and preserve the ECM when decellularization is performed using the same protocol, resulting in failure to restore airway function *in vivo*. To address this issue, an individual decellularization protocol for the separated respiratory mucosa and cartilage has been suggested.

Most previous decellularization protocols for the trachea used enzymatic methods, which are efficient but destructive to the ECM, as well as expensive [24, 25]. An ideal decellularization protocol should use decellularization agents that require less time and cost for clinical applications. The aim of this study was to develop an ideal decellularization protocol for porcine respiratory epithelium separated from the cartilage, as well as evaluate its characteristics. We applied commercial sterilizing agents comprising a compound of disodium carbonate with $H_2O_2$ (2:3) and citric acid (Rely+On Perasafe; DuPont, Wilmington, DE, USA) as decellularizing agents to realize low-cost decellularization and sterilizing effects. Our results indicate the successful development of a modified decellularization protocol for separating respiratory epithelium from cartilage.

## 2 Materials and methods

### 2.1 Trachea harvest and study design

The porcine trachea was obtained from a local abattoir from adult, market-sized pigs (~ 110–140 kg). The trachea was washed with normal saline containing 1% antibiotic and antimycotic solution (Gibco, Grand Island, NY, USA) overnight at 4 °C to remove blood clots, debris, and microorganisms. The tracheal mucosa was then divided into five groups according to the decellularization protocol (Fig. 1). The tracheal mucosa separated from cartilage after washing was defined as native group. After processing, all trachea sections were frozen at − 80 °C, except the native trachea samples. The tracheal mucosa separated after freeze–thawing was labelled freeze–thawed (FT) mucosa. Perasafe-based detergent-enzymatic decellularization protocol was applied in wFTP (protocol was applied to the unseparated trachea and then tracheal mucosa was separated) and mFTP (protocol was applied to separated tracheal mucosa) groups. DNase based detergent-enzymatic decellularization protocol was applied to separated tracheal mucosa, and this group was called the mFTD group.

### 2.2 Decellularization protocol

The trachea was thawed in a 25 °C warm bath for 30 min, after which the trachea mucosa was mechanically separated from the cartilage and analyzed as FT mucosa.

#### *2.2.1 FTD group*

Samples were incubated in a shaker (VWR International, Pittsburgh, PA, USA) at 150 rpm in the following solutions: 0.25% trypsin with 0.05% EDTA (Gibco) for 4 h at 36.5 °C; distilled water (DW) for 30 min (2 ×), DW for 1 h (2 ×), 1% Triton X-100 (Sigma-Aldrich, St. Louis, MO, USA) overnight and for another 24 h at 25 °C, DW for 30 min (2 ×), DW for 1 h (2 ×), DNase I (100 U/mL, Sigma-Aldrich) for 6 h at 37 °C followed by DW for 30 min (2 ×), and DW for 1 h (2 ×). As final washing step, samples were incubated overnight in PBS with antibiotics and antifungal solution at 4 °C.

#### *2.2.2 FTP groups (wFTP and mFTP)*

Samples were incubated in a shaker (VWR International, Pittsburgh, PA, USA) at 150 rpm in the following

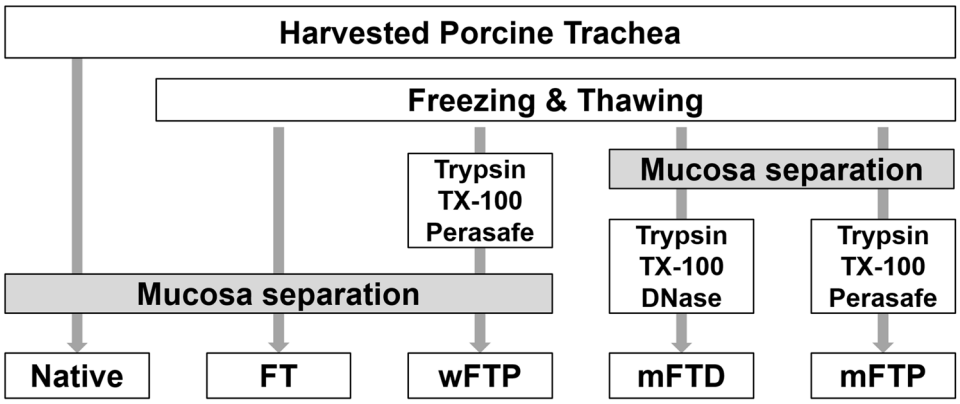


**Fig. 1** Decellularization protocol. Procine trachea was harvested and underwent decellularization protocol as above chart. The groups were divided as their protocol

solutions: 0.25% trypsin with 0.05% EDTA (Gibco) for 4 h at 36.5 °C, DW for 30 min (2 ×), DW for 1 h (2 ×), 1% Triton X-100 (Sigma-Aldrich, St. Louis, MO, USA) overnight and for another 24 h at 25 °C, DW for 30 min (2 ×), and DW for 1 h (2 ×), Perasafe® for 1 h at 25 °C, DW for 30 min (2 ×), DW for 1 h (2 ×). As final washing step, samples were incubated overnight in PBS with antibiotics and antifungal solution at 4 °C.

## 2.3 *In vitro* analysis

### *2.3.1 DNA quantification*

Total DNA content within the native tissue and decellularized tracheal samples was accessed using a DNeasy blood and tissue kit (Qiagen, Hilden, Germany) according to manufacturer instructions. Briefly, 5 mg of freeze-dried samples was digested overnight with proteinase K at 65 °C, after which DNA was isolated using the supplied buffers and mini-columns. Eluted DNA was quantified with a Quant-iT PicoGreen dsDNA assay kit (Thermo Fisher Scientific, Waltham, MA, USA). The standards and experimental DNA solution were mixed with diluted PicoGreen reagent, and fluorescence emission was measured at 520 nm in a microplate reader (Synergy H1; Biotek, Winooski, VT, USA).

### *2.3.2 Collagen quantification*

The Sircol soluble collagen assay kit (Biocolor, Carrickfergus, UK) was used to isolate and quantify the collagen content of the samples according to manufacturer instructions. Briefly, 1 mg of freeze-dried sample was hydrolyzed with 1 mL of pepsin solution (0.1 mg/mL pepsin in 0.5 M acetic acid) at 4 °C for 1 week. After neutralization, collagen was isolated using the supplied isolation and concentration reagent, after which 100 μL of the sample was added to 1 mL of colorimetric reagent and agitated for 30 min, followed by centrifugation at 19,000 g for 10 min. The dye was released from the pellet using the supplied alkali reagent, and absorbance at 555 nm was measured using a microplate reader (Synergy H1; Biotek, Winooski, VT, USA). Absolute values were obtained using a standard graph comprising the collagen type I standard supplied with the kit in the range of 5–100 μg per 0.3 mL.

### *2.3.3 Glycosaminoglycan (GAG) quantification*

Total sulfated GAG content within the native tissue and decellularized tracheal samples was quantified using a Blyscan sulfated glycosaminoglycan assay kit (Biocolor) according manufacturer instructions. Briefly, 1 mg of freeze-dried sample was digested with 1 mL of papain extraction buffer (Sigma-Aldrich) at 65 °C for 1 day, after which each tube contained 100 μL of test samples, standards, or blank. Blyscan dye reagent (1 mL) was added and mixed for 30 min using a mechanical shaker, followed by centrifugation at 12,000 rpm for 10 min. The supernatant was carefully removed, and 1 mL of dissociation reagent was added to the tubes and allowed to dissolve for 10 min before measurement. The absorbance of the reagent blanks, GAG standards, and test samples was measured at 656 nm using a microplate reader (Synergy H1; Biotek, Vermont, USA). Absolute values were obtained from a standard graph prepared using the supplied GAG standards in the range of 1–5 μg per 0.1 mL.

### *2.3.4 Histology*

Samples were fixed in 10% neutral-buffered formaldehyde (Sigma-Aldrich) for $> 24$ h and embedded in paraffin blocks, which were cut with a microtome into 4-μm-thick sections. After deparaffinization and rehydration, we conducted hematoxylin and eosin (H&E) staining to evaluate the presence of nuclei in decellularized tissue and safranin-O staining to evaluate the proteoglycan and collagen content of the tissue.

For immunohistochemistry, after deparaffinization and rehydration, the sections were rinsed three times with PBS, treated with 3% $H_2O_2$ (Sigma-Aldrich) for 5 min, and rinsed with PBS containing 0.05% Triton X-100 (PBST; Sigma-Aldrich). For antigen and epitope retrieval, the sections were incubated with pepsin solution (GBI Labs, Bothell, WA, USA) at 37 °C for 20 min and rinsed three times with PBST. Non-specific binding was blocked with pre-blocking solution (GBI Labs) for 30 min, followed by rinsing three times with PBST. The sections were incubated overnight at 4 °C with primary antibodies against collagen type I, collagen type IV, cytokeratine V, fibronectin, laminin, epidermal growth factor, fibroblast growth factor (FGF), transforming growth factor-β (TGF-β), and CD45 (leukocyte common antigen) (Origene, Rockville, MD, USA). After rinsing with PBST, the sections were incubated with biotinylated secondary antibodies (GBI Labs) for 1 h and horseradish peroxidase-streptavidin (GBI Labs) for 1 h, followed by visualization using DAB solution (GBI Labs). After staining, the sections were mounted onto gelatin-coated slides and examined under a bright-field microscope (Optinity KCS-31S; Korea Lab Tech, Seoul, Korea), with images obtained using OptiView 3.7 software (Korea Lab Tech).

#### *2.3.5 Scanning electron microscopy (SEM)*

SEM images were obtained at the luminal and cross-sectioned surfaces of the samples in order to observe morphological changes in the mucosa. Samples were fixed in 2.5% glutaraldehyde for 1 day at room temperature, followed by rinsing with distilled water and dehydration with 100% ethanol using a graded ethanol–water series. The samples were mounted onto an aluminum stub after coating with a platinum sputter coater (208HR; Cressington Scientific Instruments, Watford, UK). The images were obtained by field emission SEM (JSM-6700F; JEOL, Tokyo, Japan).

#### *2.3.6 Cytocompatibility assessment*

The cytcompatibility of the native and decellularized mucosa was examined by co-culturing tonsil-derived mesenchymal stem cells (TMSCs) with the membrane using Transwell inserts (Corning, Corning, NY, USA) with a pore size of 3 μm. Briefly, TMSCs were plated in the lower compartment, and the mucosa was placed in the upper compartment and cultured in Dulbecco's modified Eagle medium (DMEM), with a negative control prepared using DMEM alone. TMSC proliferation at 1, 2, and 3 days was measured using a EZ-Cytox cell viability assay kit (Daeil Lab Service, Seoul, Korea). The cytotoxicity of each mucosa sample was evaluated by calculating the relative growth rate [RGR = (mean optical density for each group)/(mean optical density of the negative control) × 100%] to determine the proliferation index [26].

The cytocompatibility test was performed using direct method, as described previously [13]. Briefly, native and decellularized mucosa were cut into 5-mm discs using a biopsy punch (Ellis Instrument, Madison, NJ, USA). Prior to cell seeding, the mucosa was oriented with the luminal surface side up in a 96-well plate (SPL Life Sciences, Gyeonggi-do, Korea) and incubated overnight in 200 μL of DMEM. TMSCs were seeded at $1 \times 10^4$ cells/well and allowed to adhere overnight. The mucosa was transferred to a new plate while maintaining the same orientation. Cell viability was examined after 1, 2, and 3 days using the EZ-Cytox cell viability assay kit (Daeil Lab Service).

### 2.4 *In vivo* biocompatibility assay

#### *2.4.1 Animal experiments*

Animal experiments evaluating the *in vivo* biocompatibility of the scaffolds was approved by the Committee for Ethics in Animal Experiments of Ewha Medical Research Institute. We randomly allocated 18 male C57BL/6 mice (Orient Bio, Seoul, Korea) weighing between 20 and 25 g into three groups (SHAM operation, native mucosa, and mFTP-mucosa). All animals were acclimated for at least 7 days before the experiments, housed under a 12-h light/dark cycle, and allowed free access to food and water. In all three groups, a 1-cm vertical incision was made at 0.5 cm beside the dorsum midline. A subdermal pocket was created by finger dissection, and a hydrated circular-shaped mucosa with a diameter of 8 mm was inserted, except in the SHAM group. At 3-days, 2-weeks, and 5-weeks post-operation, the mice were sacrificed, and the implanted mucosa was retrieved en bloc for histologic evaluation. The animal care complied with the Guide for the Care and Use of Laboratory Animals by the Institute of Laboratory Animal Resources and National Institutes of Health and Animal Experiment Guidelines of Ewha Womans University Medical Research Institute.

#### *2.4.2 Histological evaluation of implanted mucosa*

The retrieved implants were fixed in 4% paraformaldehyde solution (Biosesang, Seong-nam, Korea) and embedded in paraffin, followed by sectioning at 4-μm thickness. H&E staining was conducted for the slides, and *in vivo* biocompatibility was evaluated by grading the histological score of the native and FTP implanted samples at 3, 14, and 35 days according to a modified version of the previously reported semiquantitative scoring criteria (Table 1) [27, 28].

**Table 1** Histological grading of implanted scaffold

| Histological findings | 3 | 2 | 1 | 0 |
|---|---|---|---|---|
| *Day 3 scoring criteria* | | | | |
| Cellular infiltration (per 40 × field) | > 150 cells | 75–150 cells | 1–75 cells | 0 cells |
| Degradation | No scaffold present | Some scaffold present | Mostly present | No degradation |
| Encapsulation | No encapsulation | Minimal encapsulation | Moderate encapsulation | Dense encapsulation |
| Inflammatory cell aggregation (per 40× field) | 0 cells | 1–75 cells | 75–150 cells | > 150 cells |
| *Day 14 scoring criteria* | | | | |
| Cellular infiltration (per 40× field) | > 150 cells | 75–150 cells | 1–75 cells | 0 cells |
| Connective tissue organization | Highly organized connective tissue present | Moderately organized connective tissue present | Unorganized connective tissue throughout disrupted original scaffold | Original scaffold intact |
| Degradation | No scaffold present | Some scaffold present | Mostly present | No degradation |
| Encapsulation | No encapsulation | Minimal encapsulation | Moderate encapsulation | Dense encapsulation |
| Multinucleated giant cells (per 40× field) | 0 cells | 1 cell | 2–5 cells | > 5 cells |
| Vascularity (per 40× field) | > 10 vessels | 6–10 vessels | 2–5 vessels | 0–1 vessel |
| *Day 35 scoring criteria* | | | | |
| Connective tissue organization | Highly organized connective tissue present | Moderately organized connective tissue present | Unorganized connective tissue throughout disrupted original scaffold | Original scaffold intact |
| Degradation | No scaffold present | Some scaffold present | Mostly present | No degradation |
| Encapsulation | No encapsulation | Minimal encapsulation | Moderate encapsulation | Dense encapsulation |
| Multinucleated giant cells (per 40× field) | 0 cells | 1 cell | 2–5 cells | > 5 cells |

### 2.5 Statistical analysis

A Wilcoxon signed-rank test was used to determine differences in dsDNA weight, GAG content, collagen content, cell viability, and proliferation results between experimental groups, with a $p < 0.05$ considered statistically significant. Statistical analysis was performed using SPSS software (v19; IBM Crop., Armonk, NY, USA). All data are reported as the mean ± standard error of the mean.

## 3 Results

### 3.1 Characteristics of decellularized porcine tracheal mucosa

#### *3.1.1 Decellularization efficacy*

The decellularization efficacy of each protocol was analyzed using established guidelines [29]. The DNA content of scaffolds was significantly reduced ($p < 0.01$) after the decellularization procedure (< 50 ng/mg) as compared with that in the native and FT groups (3996.8 ± 1810.2 ng/mg and 2524.8 ± 568.1 ng/mg, respectively) (Fig. 2A). Intact nuclei were not observed according to H&E staining in the wFTP, mFTD, or mFTP groups (Fig. 2B), and CD45 stain was negative in mFTD and mFTP groups, however, wFTP groups demonstrated positive stain, which means remained antigenicity of the specimen (Fig. 2C).

#### *3.1.2 Biochemical and microstructural composition of decellularized tracheal mucosa*

The concentration of collagen in the detergent-enzymatic decellularization protocol groups (wFTP, mFTD, and mFTP) did not decrease relative to that observed in the native and FT groups ($p > 0.05$), with between-group comparisons indicating that collagen concentration in the mFTP groups was lower than that in the wFTP and mFTD groups. Additionally, GAG concentrations differed

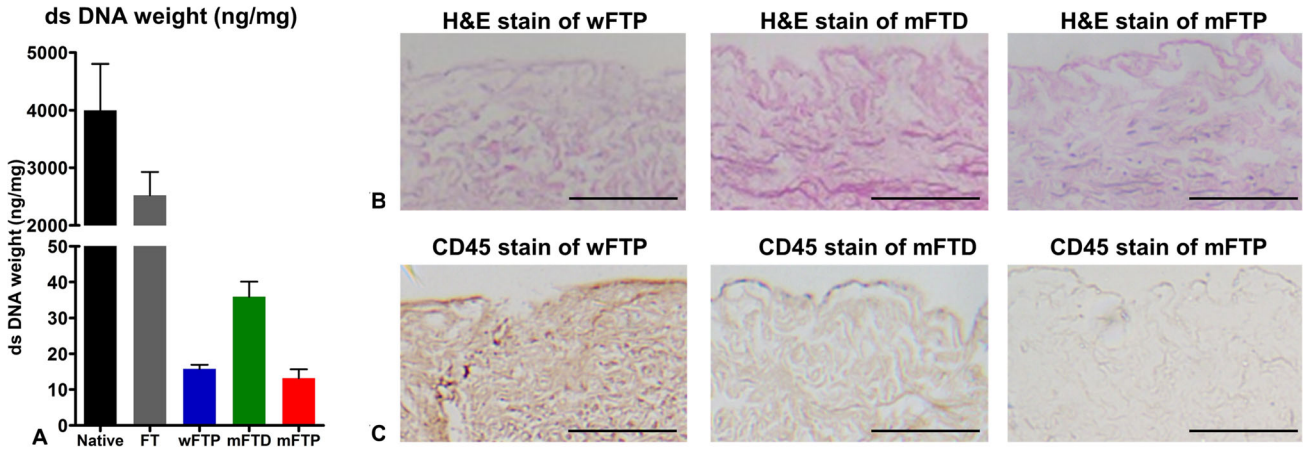


**Fig. 2** Decellularization efficacy. **A** The dsDNA dry weights of wFTP, mFTD, and mFTP mucosa were less than 50 ng/mg. **B** No intact nuclei were observed on wFTP, mFTD, and mFTP protocol decellularization group by H&E stain. **C** CD 45 was only positively stained in wFTP mucosa, and not positively stained in mFTD and mFTP mucosa

significantly between the native group and each experimental group ($p \leq 0.05$). These results indicated no significant difference between the decellularized groups (Fig. 3).

Safranin-O staining revealed that the collagen fibers remained after the decellularization protocols. Immunohistochemical staining to evaluate ECM distribution (collagen I, collagen IV, cytokeratin V, fibronectin, and laminin) revealed that only fibronectin was remained after decellularization protocol, but the other ECM decreased a lot, only weakly stained positive stains were observed. Additionally, vascular endothelial growth factor (VEGF) was positive throughout the decellularized area after the decellularization protocol, whereas TGF-β and FGF levels were greatly decreased as compared with those in the native group (Fig. 4). SEM images of the luminal side of the scaffold showed a smooth surface. Images of the cross-sectioned side of the scaffold showed a more fibrous and porous structure, which is advantageous for cellular attachment (Fig. 5).

### 3.1.3 *Biocompatibility of the decellularized mucosa*

Compared with controls (TMSCs cultured with media alone), TMSC viability measured at 1, 2, and 3 days demonstrated no apparent differences in RGRs between the experimental and control groups when cultured using a Transwell insert. We evaluated TMSC growth on the mucosa by plating cells on the mucosa, followed by culture for 1, 2, and 3 days in DMEM, with mucosa without seeded cells used as a negative control for each group. We used TMSC viability measured at 1, 2, and 3 days to estimate cell adhesion and growth on each type of mucosa. Our data showed that the decellularized-mucosa groups supported significantly higher TMSC growth ($p < 0.01$) than that observed in the native and FT mucosa groups. Among the decellularized-mucosa groups, TMSCs exhibited improved proliferation on mFTP mucosa than on mFTD mucosa (Fig. 6).

Semiquantitative scoring of *in vivo* samples revealed that the mFTP mucosa displayed a higher degree of biocompatibility relative to that of native mucosa (total scores of 21.5 and 14.5, respectively) (Table 2). Moreover, acute inflammatory cell aggregation was more dominant in

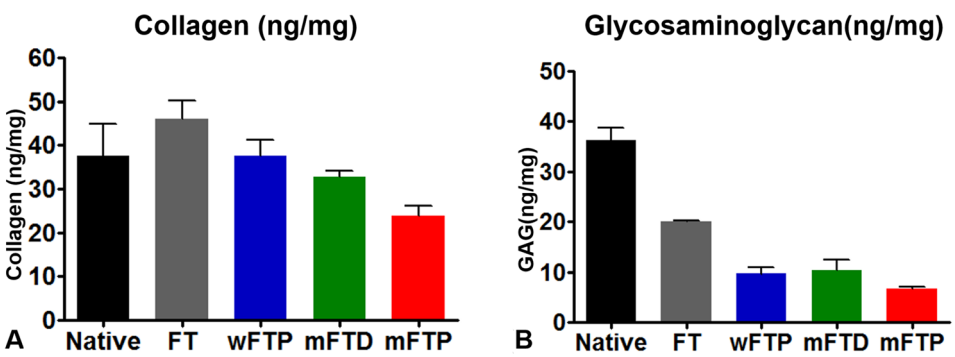


**Fig. 3** Collagen and glycosaminoglycan contents. **A** Collagen contents were decreased after the decellularization. **B** Glycosaminoglycan decreased significantly after chemical-enzymatic process. There was no significant difference between the three groups (wFTP, mFTD, and mFTP)

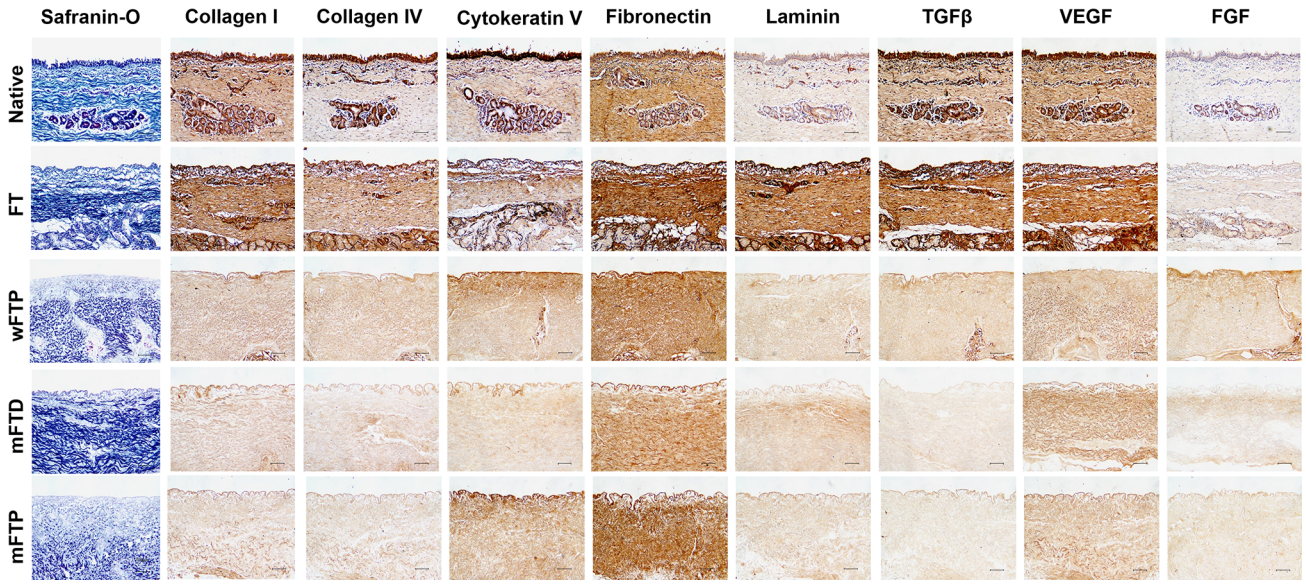


**Fig. 4** Histological finding of the scaffolds. Safranin O stain revealed that collagen (blue stain). Dark brown indicated positive stain in immunolabeling. Scale bar = 100 μm

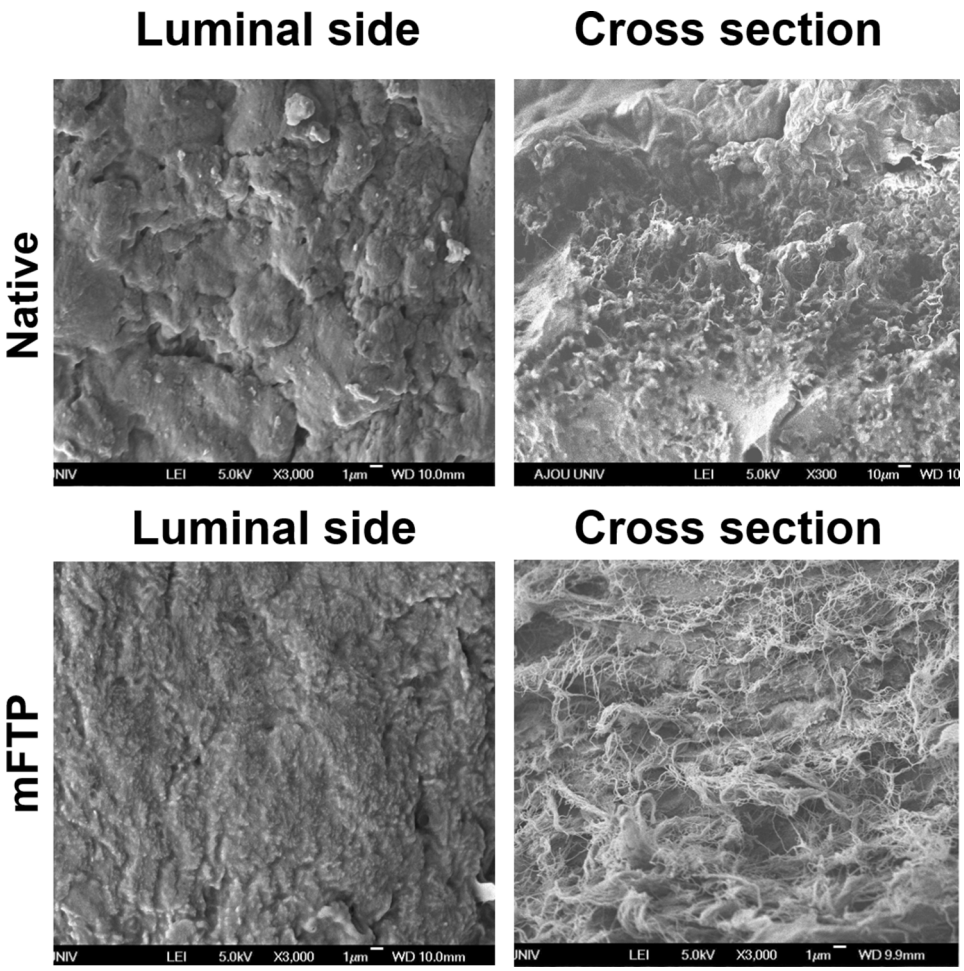


**Fig. 5** Scanning electron microscope (SEM) evaluation of native and mFTP scaffold. The luminal surface of the native and mFTP scaffolds was smooth and cross-sectional space has microporous ultrastructure. Scale bar = 1 μm

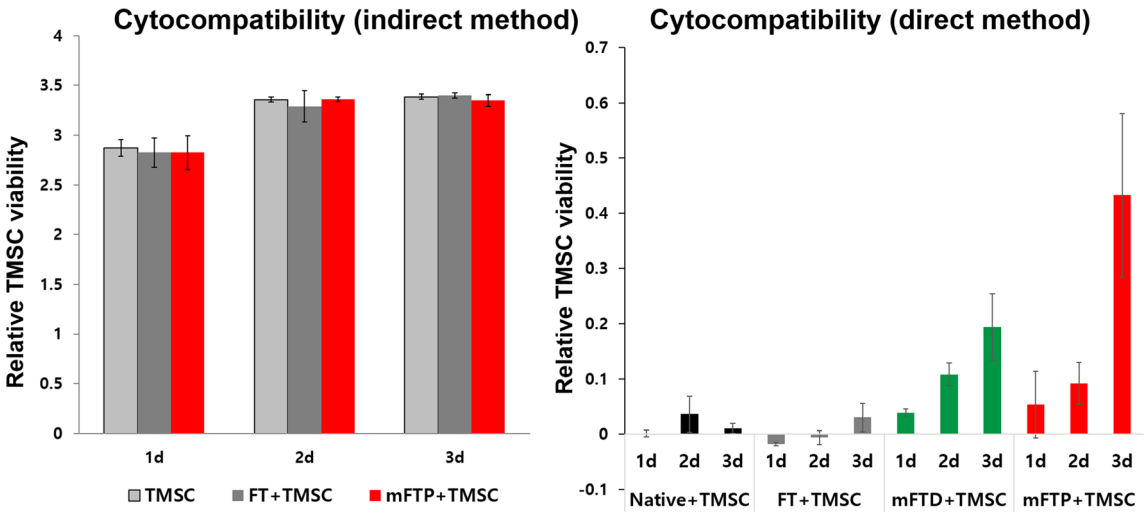


**Fig. 6** *In vitro* biocompatiblity. **A** Cytocompatibility assay using indirect method revealed that culture medium with scaffold showed no cytotoxicity when compared with culture medium without scaffold. **B** The cell viability of tonsil-derived mesenchymal stem cells (TMSCs) after 24, 48, and 72 h-culture on freeze–thaw scaffold, mFTP scaffold, and tissue culture plastic was assessed

**Table 2** Histological grading results of implanted scaffold

| Histological findings | Native mucosa | mFTP mucosa |
|---|---|---|
| *Day 3 scoring criteria* | | |
| Cellular infiltration (per 40× field) | 1 | 1.5 |
| Degradation | 0 | 0 |
| Encapsulation | 2 | 1.5 |
| Inflammatory cell aggregation (per 40× field) | 3 | 1.5 |
| *Day 14 scoring criteria* | | |
| Cellular infiltration (per 40× field) | 1 | 0 |
| Connective tissue organization | 1 | 1 |
| Degradation | 0 | 0 |
| Encapsulation | 3 | 2 |
| Multinucleated giant cells (per 40× field) | 2 | 3 |
| Vascularity (per 40× field) | 0 | 0 |
| *Day 35 scoring criteria* | | |
| Connective tissue organization | 2 | 1 |
| Degradation | 1 | 0 |
| Encapsulation | 2.5 | 1 |
| Multinucleated giant cells (per 40× field) | 3 | 2 |
| Total | 21.5 | 14.5 |

native-mucosa-implanted group at 3 days. Evaluation of long-term inflammatory reactions indicated that multinucleated giant cells and encapsulation of the implanted scaffold were more frequently observed in native-mucosa-embedded groups at 35 days, whereas the connective tissue of implanted mFTP was organized and cellular infiltration observed at the same time point (Fig. 7).

## 4 Discussion

The advantage of using site-specific biological scaffolds is that they provide a favorable environment for tissue regeneration [30–32]. Remaining ECM in the scaffold plays a key role by forming a microenvironmental niche; however, scaffolds that are not fully decellularized or contain toxic chemicals originating from decellularizing agents are harmful to tissue regeneration [33, 34].

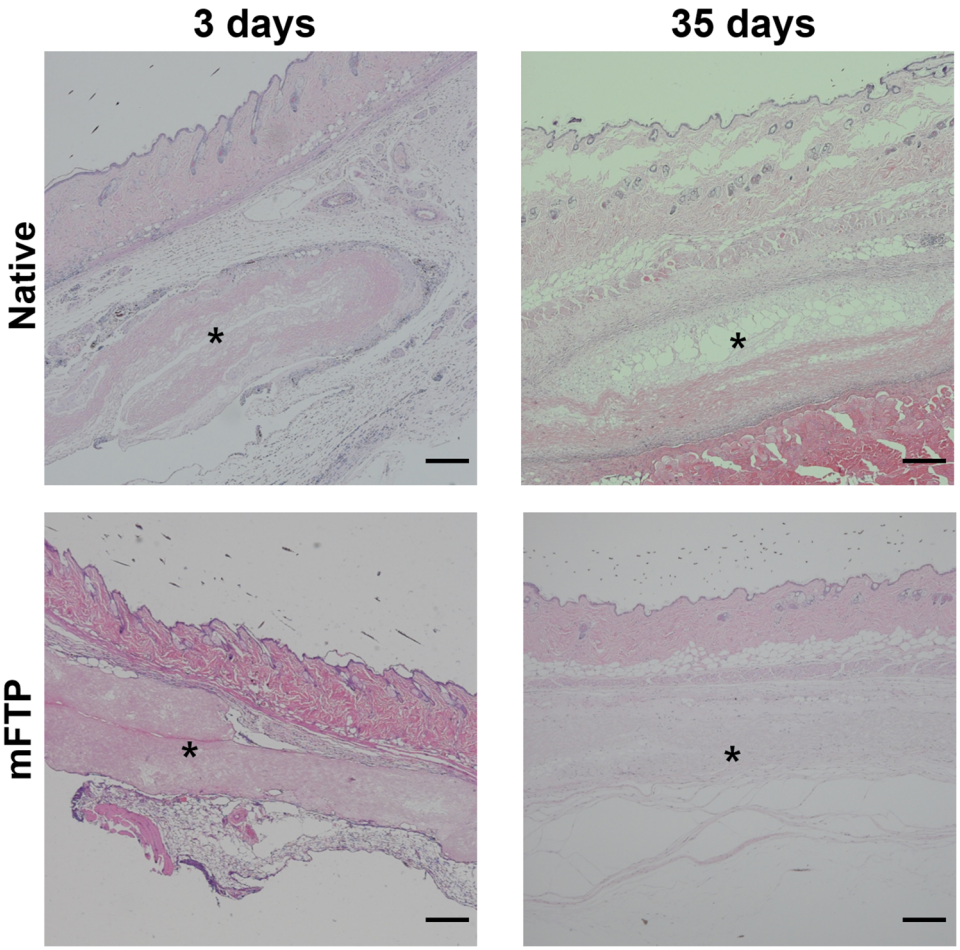


**Fig. 7** *In vivo* biocompatiblity. H&E stain image of the implanted mucosa (native and mFTP group, 3 days and 35 days after implantation). Implanted mucosa (asterisk) was surround by neutrophils in 3 days, especially in native group. After 35 days, cellular infiltration was observed in mFTP mucosa while fewer cellular infiltration and necrosis of the implanted mucosa was noticed in native mucosa. Scale bar = 500 μm

Therefore, an efficient decellularization protocol for each tissue is very important.

In this study, acellular respiratory mucosal matrix (ARMM) produced by the decellularization protocol showed the proper decellularization status, with dsDNA weight at $< 50$ ng/mg and no nuclei observed according to H&E staining. Comparison of each protocol indicated that mFTP (separated tracheal mucosa with Perasafe) mucosa showed the lowest dsDNA weight (wFTP, wFTD, and mFTP ranges: 5.4–31.7, 25.8–51.0, and 1.3–27.8 ng/mg, respectively). Additionally, CD45 staining revealed that the mFTP mucosa showed very low antigenicity as compared with wFTP mucosa. To determine the cytotoxicity of the decellularized mucosa, we examined TMSC growth in the presence of mucosa using a Transwell insert, with our results indicating no apparent cytotoxicity in the mFTP group. These results indicated that the decellularization protocol using Perasafe on the separated mucosa was highly efficient and safe.

An ideal scaffold should promote cell adhesion and growth. Evaluation of TMSC growth on the wFTP scaffold showed that wFTP scaffolds supported significantly higher levels of TMSC growth ($p < 0.01$) relative to the other groups. This is likely because the mFTP scaffold has a proper microstructure that allows the ECM to facilitate cellular ingrowth. SEM evaluation of the ECM microstructure showed a cross-sectional view revealing a porous structure, which is advantageous for cell attachment. Assessment of the ECM composition of the ARMMs revealed that the wFTP protocols displayed an ECM-preservation capacity comparable to protocols using DNase as a final agent. Additionally, the collagen concentration was lower in the mFTP group relative to that in the mFTD and wFTP groups according to quantitative comparison; however, GAG concentration did not differ significantly between groups. Moreover, immunohistochemical staining revealed preservation of collagen IV, cytokerain V, fibronectin, and VEGF after the decellularization protocol using the separated tracheal mucosa. These preserved structures facilitate connective-tissue organization, as demonstrated by semiquantitative histologic grades using H&E staining of the implanted scaffolds.

These results demonstrated the potential of applying a decellularization protocol using trachea mucosa alone. This is the first study describing decellularization of separated tracheal mucosa, and showing that separation of the

mucosa from the cartilage allows the avoidance of excessive cartilage-decellularization steps. Therefore, the protocols described here enable proper decellularization of the mucosa. Furthermore, because the ARMMs were produced as a sheet, this method can easily be applied in the clinical field and not only for tracheal mucosal defects but also for other airway mucosal defects, such as those in the nasal cavity, sinus, and middle ear mucosa.

One significant advantage of this protocol is its low cost. For clinical use, the production cost of the ARMM should be reasonable; therefore, we used a commercialized compound of disodium carbonate and a compound with $H_2O_2$ (Perasafe) as a decellularization agent. A cost comparison of this protocol with a tracheal-decellularization protocol using DNase revealed a significant decrease in the cost of preparing 400 mL of decellularization solution (347,000 won vs. 1924 won). Furthermore, the amount of tracheal mucosa retrieved from one cadaver donor is very limited; therefore, porcine trachea is the most appropriate source for mass production due to its size, availability, and cost.

For clinical applications, additional studies should be performed. The sterilizing status evaluation and toxicity assay for chemical agent which was used for decellularization should be performed. We evaluated the biocompatibility by means of ectopic transplantation to small animal dorsum. As the airway mucosa is exposed to the air and mucus in nature, the biocompatibility study using orthotopic implantation should be conducted. Additionally, studies are necessary to evaluate ability of the scaffold in facilitating the respiratory mucosal regeneration using the airway-mucosal defect in large animal.

In the study, we described the development of a novel ARMM by applying a decellularization protocol using a commercialized compound of disodium carbonate and $H_2O_2$ to separate the porcine tracheal respiratory epithelium. This ARMM showed suitable antigenicity status and demonstrated a proper ECM for use as a biocompatible scaffold. For clinical use, this scaffold displayed the advantages of sheet-type features and low production costs.

**Acknowledgements** This study was supported by 2016 Young Medical Science Researcher Grants from Ewha Womans University College of Medicine and grants from the Basic Science Research Program through the National Research Foundation of Korea funded by the Ministry of Education, Science and Technology (Grant No. NRF-2017R1D1A1B03034399).

**Compliance with ethical standards**

**Conflict of interest** The authors have no conflicts of interest to disclose.

**Ethical statement** The animal studies were performed after receiving approval of the Institutional Animal Care and Use Committee in Ewha Womans University Medical Research Institute (Approval No. ESM-.18-0404).

## References

1. Tsukada H, Osada H. Experimental study of a new tracheal prosthesis: pored Dacron tube. J Thorac Cardiovasc Surg. 2004;127:877–84.
2. Kim HS, Suh H, Lee JH, Kim JH, Song DE, Jo I, et al. Development of an artificial tracheal prosthesis: a semicircular shape polyurethane scaffold. Tissue Eng Regen Med. 2011;8:439–45.
3. Chang JW, Park SA, Park JK, Choi JW, Kim YS, Shin YS, et al. Tissue-engineered tracheal reconstruction using three-dimensionally printed artificial tracheal graft: preliminary report. Artif Organs. 2014;38:E95–105.
4. Hong HJ, Chang JW, Park JK, Choi JW, Kim YS, Shin YS, et al. Tracheal reconstruction using chondrocytes seeded on a poly(L-lactic-*co*-glycolic acid)-fibrin/hyaluronan. J Biomed Mater Res A. 2014;102:4142–50.
5. Lee JH, Park HS, Oh SH, Lee JH, Kim JR, Kim HJ, et al. Triple-layered polyurethane prosthesis with wrinkles for repairing partial tracheal defects. Laryngoscope. 2014;124:2757–63.
6. Melgoza EL, Vallicrosa G, Serenó L, Ciurana J, Rodríguez AC. Rapid tooling using 3D printing system for manufacturing of customized tracheal stent. Rapid Prototyp J. 2014;20:2–12.
7. Shin YS, Lee BH, Choi JW, Min BH, Chang JW, Yang SS, et al. Tissue-engineered tracheal reconstruction using chondrocyte seeded on a porcine cartilage-derived substance scaffold. Int J Pediatr Otorhinolaryngol. 2014;78:32–8.
8. Chua M, Chui CK, Teo C, Lau D. Patient-specific carbon nanocomposite tracheal prosthesis. Int J Artif Organs. 2015;38:31–8.
9. Park JH, Hong JM, Ju YM, Jung JW, Kang HW, Lee SJ, et al. A novel tissue-engineered trachea with a mechanical behavior similar to native trachea. Biomaterials. 2015;62:106–15.
10. Shin YS, Choi JW, Park JK, Kim YS, Yang SS, Min BH, et al. Tissue-engineered tracheal reconstruction using mesenchymal stem cells seeded on a porcine cartilage powder scaffold. Ann Biomed Eng. 2015;43:1003–13.
11. Jung SY, Lee SJ, Kim HY, Park HS, Wang Z, Kim HJ, et al. 3D printed polyurethane prosthesis for partial tracheal reconstruction: a pilot animal study. Biofabrication. 2016;8:045015.
12. O'Leary C, Cavanagh B, Unger RE, Kirkpatrick CJ, O'Dea S, O'Brien FJ, et al. The development of a tissue-engineered tracheobronchial epithelial model using a bilayered collagen-hyaluronate scaffold. Biomaterials. 2016;85:111–27.
13. Butler CR, Hynds RE, Crowley C, Gowers KH, Partington L, Hamilton NJ, et al. Vacuum-assisted decellularization: an accelerated protocol to generate tissue-engineered human tracheal scaffolds. Biomaterials. 2017;124:95–105.
14. Baiguera S, Jungebluth P, Burns A, Mavilia C, Haag J, De Coppi P, et al. Tissue engineered human tracheas for in vivo implantation. Biomaterials. 2010;31:8931–8.
15. Partington L, Mordan NJ, Mason C, Knowles JC, Kim HW, Lowdell MW, et al. Biochemical changes caused by decellularization may compromise mechanical integrity of tracheal scaffolds. Acta Biomater. 2013;9:5251–61.
16. Zang M, Zhang Q, Chang EI, Mathur AB, Yu P. Decellularized tracheal matrix scaffold for tracheal tissue engineering: in vivo host response. Plast Reconstr Surg. 2013;132:549e–59.
17. Sun F, Pan S, Shi HC, Zhang FB, Zhang WD, Ye G, et al. Structural integrity, immunogenicity and biomechanical evaluation of rabbit decelluarized tracheal matrix. J Biomed Mater Res A. 2015;103:1509–19.
18. Den Hondt M, Vanaudenaerde BM, Maughan EF, Butler CR, Crowley C, Verbeken EK, et al. An optimized non-destructive protocol for testing mechanical properties in decellularized rabbit trachea. Acta Biomater. 2017;60:291–301.

19. Xu Y, Li D, Yin Z, He A, Lin M, Jiang G, et al. Tissue-engineered trachea regeneration using decellularized trachea matrix treated with laser micropore technique. Acta Biomater. 2017;58:113–21.
20. Park JH, Jung JW, Kang HW, Joo YH, Lee JS, Cho DW. Development of a 3D bellows tracheal graft: mechanical behavior analysis, fabrication and an in vivo feasibility study. Biofabrication. 2012;4:035004.
21. Chua CHM, Chui CK, Rai B, Lau DPD. Development of a patient specific artificial tracheal prosthesis: design, mechanical behavior analysis and manufacturing. Conf Proc IEEE Eng Med Biol Soc. 2013;2013:6236–9.
22. Macchiarini P, Jungebluth P, Go T, Asnaghi MA, Rees LE, Cogan TA, et al. Clinical transplantation of a tissue-engineered airway. Lancet. 2008;372:2023–30.
23. Delaere P, Vranckx J, Verleden G, De Leyn P, Van Raemdonck D, Leuven Tracheal Transplant Group. Tracheal allotransplantation after withdrawal of immunosuppressive therapy. N Engl J Med. 2010;362:138–45.
24. Gui L, Chan SA, Breuer CK, Niklason LE. Novel utilization of serum in tissue decellularization. Tissue Eng Part C Methods. 2010;16:173–84.
25. Hussein KH, Park KM, Kang KS, Woo HM. Biocompatibility evaluation of tissue-engineered decellularized scaffolds for biomedical application. Mater Sci Eng C Mater Biol Appl. 2016;67:766–78.
26. Xu S, Lu F, Cheng L, Li C, Zhou X, Wu Y, et al. Preparation and characterization of small-diameter decellularization scaffolds for vascular tissue engineering in an animal model. Biomed Eng Online. 2017;16:55.
27. Keane TJ, Londono R, Carey RM, Carruthers CA, Reing JE, Dearth CL, et al. Preparation and characterization of a biologic scaffold from esophageal mucosa. Biomaterials. 2013;34:6729–37.
28. Valentin JE, Badylak JS, McCabe GP, Badylak SF. Extracellular matrix bioscaffolds for orthopaedic applications: a comparative histologic study. J Bone Joint Surg Am. 2006;88:2673–86.
29. Crapo PM, Gilbert TW, Badylak SF. An overview of tissue and whole organ decellularization processes. Biomaterials. 2011;32:32–43.
30. Allen RA, Seltz LM, Jiang H, Kasick RT, Sellaro TL, Badylak SF, et al. Adrenal extracellular matrix scaffolds support adrenocortical cell proliferation and function in vitro. Tissue Eng Part A. 2010;16:3363–74.
31. French KM, Boopathy AV, DeQuach JA, Chingozha L, Lu H, Christman KL, et al. A naturally derived cardiac extracellular matrix enhances cardiac progenitor cell behavior in vitro. Acta Biomater. 2012;8:4357–64.
32. Sellaro TL, Ravindra AK, Stolz DB, Badylak SF. Maintenance of hepatic sinusoidal endothelial cell phenotype in vitro using organ-specific extracellular matrix scaffolds. Tissue Eng. 2007;13:2301–10.
33. Morris AH, Chang J, Kyriakides TR. Inadequate processing of decellularized dermal matrix reduces cell viability in vitro and increases apoptosis and acute inflammation in vivo. Biores Open Access. 2016;5:177–87.
34. Wong ML, Griffiths LG. Immunogenicity in xenogeneic scaffold generation: antigen removal vs. decellularization. Acta Biomater. 2014;10:1806–16.